Predicting Unsteady Solute Transport through Green Stormwater Infrastructure with

Transit Time Distribution Theory

E.A. Parker, S.B. Grant, Y. Cao, M.A. Rippy, K. McGuire, P. Holden, M. Feraud, S. Avasarala, H. Liu, W. Hung, M. Rugh, J. Jay, J. Peng, S. Shao, D. Li

Contents of this file

Introduction. This Supporting Information includes a detailed description of how we estimated crop potential evapotranspiration (**Text S1**). Next, we describe our numerical evaluation of the biofilter bucket hydrology model (**Text S2**) and describe how we estimated saturated hydraulic conductivity (**Text S3**). We also provide detailed derivations (and illustrate their numerical application) for age-ranked storage under uniform selection (**Text S4**), the age structure of water in the biofilter (**Text S5**), and TTD theory predictions for reactive solute transport (**Text S6**). We then describe how the fraction of inflow that undergoes lateral exfiltration was estimated using both steady-state and transient experiments (**Text S7**). We describe how we corrected experimental timestamps so that the modeled and measured outflow volumes and concentrations aligned (**Text S8**), and document key differences between the experimental storms carried out during the summer of 2018 and 2019 (**Text S9**). References are summarized at the end of the document.

Text S1. Estimating Crop Potential Evapotranspiration (cPET)

Crop Potential Evapotranspiration (cPET) was estimated outside of Hydrus using the Penman-Monteith equation (Allen et al., 1998; FAO-56):

$$pET = \frac{1}{\lambda \rho_w} \frac{\Delta(R_n - G) + \rho_a c_p \frac{(e_s - e_a)}{r_a}}{\Delta + \gamma \left(1 + \frac{r_s}{r_a}\right)} \tag{1-1}$$

Here, R_n = net radiation (calculated, not measured, as a function of albedo, latitude and longitude, and climate variables; average temperature, relative humidity, and solar radiation), r_s = surface resistance (a function of stomatal conductance, and the leaf area index; LAI), r_a = atmospheric resistance (a function of plant height, wind speed, and the height at which wind speed and relative humidity measurements were made), G = the soil heat flux (a function of solar radiation and R_n), $e_s - e_a$ = the pressure deficit of the air (a function of temperature and relative humidity), Δ = the slope of the saturation vapor pressure temperature relationship, ρ_a = the mean air density at the elevation of the biofilter, ρ_w = the mean water density at constant pressure, c_p = the specific heat of air, γ = the psychometric constant, and λ = the latent heat of water. Each of the above-noted parameters was estimated, using the procedure described in Allen et al. (1998), at an hourly time step over the two time periods (June 25-29 in 2018, and June 1-5 in 2019) when biofilter challenge experiments were conducted at the Orange County Public Works LID Campus, City of Orange, Orange County, California. Data resources included the following. Temperature and wind speed data (sensor height: 3.7 m; back adjusted to 2 m as per Allen et al., 1998) were sourced from the onsite weather station at Orange County Public Works. Solar radiation, and relative humidity data were sourced from CIMIS station 75 located ~ 19.34 km SE of Orange County Public Works. Plant trait information appropriate for *Carex sp* was used in lieu of standard FAO values for a well-watered turf grass, and included the following. Maximum stomatal conductance was set to 0.45 mol $H_2O/m^2/s$ based on measured values for *Carex hirta*, a *Carex* species capable of tolerating the range of dry and wet soil conditions typical of stormwater biofilters (Busch & Losch, 1998). LAI was set to 1.265, an average value from four *Carex* species evaluated by Aerts et al., 1992 (min LAI: 0.75, max LAI: 2.49). Plant height was set to 0.41m, the average height of *Carex* plants in the 2019 biofilter experiments. The standard FAO value for albedo (0.23) was used as *Carex*-specific estimates for albedo were unavailable (Allen et al., 1998).

Text S2. **Numerical Solution of the Biofilter Bucket Hydrology Model.** To numerically integrate the bucket hydrology model over the 17 experimental storms carried out during the summers of 2018 and 2019, we substituted the closure relationships for infiltration, discharge, and ET into the volume balance equation (equation (1a) in the main text):

$$\frac{dS(t)}{dt} = \left\{ \begin{array}{l} I(t),\ 0 < S(t) < S_{max} \\ K_{sat},\ S(t) = S_{max} \end{array} \right\} - K_{sat}\left(\frac{S(t) - S_{min}}{S_{max}}\right)^{g} - cPET(t),\ 0 \le S(t) \le S_{max} \tag{2-1a}$$

$$S(t=0) = S_0 \tag{2-1b}$$

Terms on the righthand side were determined as follows:

- Inflow to the ponding zone, $I(t)$, was measured based on the change in weight of the inflow tank (Section 3.1, main text);

- The maximum storage, $S_{max} = 0.246$ m, was calculated from the depth and porosity of the experimental biofilter, or inferred by minimizing the root mean square error between model predicted and measured bromide concentrations (Section 4.4, main text);

- The saturated hydraulic conductivity, K_{sat}, was determined from in situ measurements and measurements of peak outflow (Text S3);

- The gravitational discharge parameters, $S_{min} = 0$ m and $g = 5.0$, were estimated by calibrating Kirchner's recessional streamflow model to Hydrus 1D simulations (Section 4.2, main text).

- cPET was estimated from local environmental measurements using FAO guidelines (Text S1).

- Finally, the initial storage, $S_0 = 0.054$ m, is equal to Hydrus 1D default values for the field capacity of loamy sand (assuming a depth and porosity of $d_b = 0.6$ m and $\theta_s = 0.41$).

Numerical integration of equation (2-1a) was carried out using the NDSolve command in Mathematica as follows (in this particular implementation there are two saturated hydraulic conductivities: ksat1 (which applies from t=0 to t=tswitch) and ksat2 (which applies from t=tswitch to t=tend), and sIC is the initial storage):

```
SVal[tend_, satIC0_, smax0_, g0_, ksat1_, ksat2_, tswitch0_] :=
 Module[{t = tend, sIC = satIC0 smax0, smax = smax0, g = g0, kstart = ksat1, kend = ksat2, tswitch = tswitch0},
  Print[smax, ", ", sIC];
  NDSolve[{s'[u] == (1 - a[u]) (inflowinterp[u] - etinterp[u] - (ksat[u] (s[u] / smax)^g)),
    p'[u] == a[u] (inflowinterp[u] - ksat[u]), q[u] == (ksat[u] (s[u] / smax)^g), ksat[0] == kstart,
    q[0] == 0, a[0] == 0, p[0] == 0, s[0] == sIC, WhenEvent[s[u] > smax, a[u] → 1],
    WhenEvent[u > tswitch, {ksat[u] -> kend}], WhenEvent[p[u] < 0, {a[u] → 0, p[u] → 0}]},
   {a, s, p, q, ksat}, {u, 0, t}, DiscreteVariables → {a, ksat}]]
```

Text S3. Estimating Saturated Hydraulic Conductivity from Measured Biofilter Outflow

During the set of experiments conducted during the summer of 2018, peak flow rates measured at the outflow tank systematically declined from approximately 0.11 m h^{-1} (first two storms) to 0.09 m h^{-1} (next four storms) to 0.08 m h^{-1} (final four storms). For the set of experiments conducted in 2019, the peak flow rates declined from approximately 0.12 m h^{-1} (first two storms) to 0.08 m h^{-1} (final five storms).

Accounting for the fraction of water recovered in 2018 and 2019 ($\alpha = 0.46 \pm 0.04$) (see Text S6) the implied saturated hydraulic conductivity values (under the assumption that the maximum outflow is equal to the saturated hydraulic conductivity (Durner & Iden, 2011; Mallants et al., 1997)) are K_{sat} = 0.24, 0.20, 0.17 m h^{-1} (first two, next four, and final four storms in 2018) and K_{sat} = 0.26 and 0.17 m h^{-1} (first two and final five storms in 2019). These K_{sat} values are consistent with eleven in situ measurements carried out during the 2019 experiments with a Philip-Dunne Infiltrometer ($K_{sat} = 0.22 \pm 0.62$ m h^{-1}) and in the range of Hydrus 1D's default value for loamy sand (0.146 m h^{-1}) (Hydrus 1D, Version 4.17.0140, PC-Progress, Prague, Czech Republic). The consistent decline in saturated hydraulic conductivity observed across the storm events simulated in the summers of 2008 and 2009 could be caused by one or more well-known processes that tend to reduce saturated hydraulic conductivity, including compaction caused by the repeated wetting and drying of sediments (c.f., Mapa et al., 1986) and the clogging of biofilter media by suspended particles in the stormwater and sewage influent mixtures (Lindsey et al., 1992; Le Coustumer et al., 2012).

Text S4. Derivation and Implementation of TTD Theory Solutions Under Uniform Selection.
Derviation of the Solution for Age-Ranked Storage. Substituting the uniform rSAS function into the conservation equation for age-ranked storage (equations (5b) and (4a), respectively, in the main text) we arrive at the governing partial differential equation to be solved where the superscript "U" denotes a uniform rSAS function:

$$\frac{\partial S_T^U}{\partial t} = J(t) - \left(f_Q(t) + f_{ET}(t)\right)S_T^U(T,t) - \frac{\partial S_T^U}{\partial T} \tag{4-1a}$$

$$f_Q(t) = \frac{Q(t)}{S(t)} \tag{4-1b}$$

$$f_{ET}(t) = \frac{ET(t)}{S(t)} \tag{4-1c}$$

$$S_T^U(T,t=0) = S_0 H(T - T_0) \tag{4-1d}$$

$$H(x) = \begin{cases} 0, & x < 0 \\ 1, & x > 0 \end{cases} \tag{4-1e}$$

$$S_T^U(T=0,t) = 0 \tag{4-1f}$$

The boundary condition (equation (4-1f)) ensures that no water volume stored in the biofilter has an age less than or equal to zero, $T = 0$. For the initial condition, equation (4-1d), all of the volume of water

initially in storage, S_0 [L], has a single age, $T = T_0$, where the function $H(x)$ (equation (4-1e)) is the Heaviside or step function. To solve the age conservation equation we begin by taking the Laplace transform of equations (4-1a) and (4-1d) with respect to the age variable, where $\tilde{S}_T$ is the Laplace image function of S_T, the independent variable p [T^{-1}] is the Laplace transform variable and the initial condition (equation (4-1f)) has been incorporated into equation (4-2a):

$$\frac{d\tilde{S}_T^U}{dt} = \frac{J(t)}{p} - \left(f_Q(t) + f_{ET}(t) + p \right) \tilde{S}_T^U(p,t) \tag{4-2a}$$

$$\tilde{S}_T^U(p,t=0) = S_0 \frac{e^{-pT_0}}{p} \tag{4-2b}$$

These last two equations can be readily integrated to yield an exact solution for age-ranked storage in the Laplace domain:

$$\tilde{S}_T^U(p,t) = e^{-\bar{f}_Q(t)-\bar{f}_{ET}(t)} \left[\frac{S_0 e^{-p(t+T_0)}}{p} + \int_0^t \frac{e^{-p(t-v)}}{p} e^{\bar{f}_Q(v)+\bar{f}_{ET}(v)} J(v) dv \right] \tag{4-3a}$$

$$\bar{f}_Q(t) = \int_0^t f_Q(u) du \tag{4-3b}$$

$$\bar{f}_{ET}(t) = \int_0^t f_{ET}(u) du \tag{4-3c}$$

The functions $\bar{f}_Q(x)$ and $\bar{f}_{ET}(x)$ represent the cumulative volume that left the biofilter by outflow and ET, respectivelym as of time t. Taking the inverse Laplace Transform of equation (4-3a) yields the following exact time-domain solution for age-ranked storage in the biofilter:

$$S_T^U(T,t) = e^{-\bar{f}_Q(t)-\bar{f}_{ET}(t)} \left[S_{fc} H(T-t-T_i) + \int_0^t H(T+v-t) e^{\bar{f}_Q(v)+\bar{f}_{ET}(v)} J(v) dv \right] \tag{4-4}$$

Numerical Implementation of the Exact Solution for Age-Ranked Storage. As a first step toward implementing this solution, the Heaviside function inside the integral term on the right hand side of equation (4-4) should be removed. Because the upper limit of the integral is greater than zero, $t > 0$, this integral can be rewritten as follows:

$$\int_0^t H(T+v-t) e^{\bar{f}_Q(v)+\bar{f}_{ET}(v)} J(v) dv = H(T-t) \int_0^t e^{\bar{f}_Q(v)+\bar{f}_{ET}(v)} J(v) dv + H(t-T) \int_{t-T}^t e^{\bar{f}_Q(v)+\bar{f}_{ET}(v)} J(v) dv$$

Substituting into equation (4-4) we arrive at the form of the age-ranked storage solution that appears in the main text (equation (6a)):

$$S_T^U(T,t) = e^{-\bar{f}_Q(t)-\bar{f}_{ET}(t)}\left[S_0 H(T-t-T_0) + \int_a^t e^{\bar{f}_Q(v)+\bar{f}_{ET}(v)} J(v)\,dv\right]$$ (4-5a)

$$a = \begin{cases} 0, & T-t>0 \\ t-T, & T-t<0 \end{cases}$$ (4-5b)

Evaluation of equation (4-5a) requires estimating the functions $\bar{f}_Q(t)$ and $\bar{f}_{ET}(t)$ (see equations (4-3b) and (4-3c)) and the integral term on the right hand side of equation (4-5a). We consider these in turn.
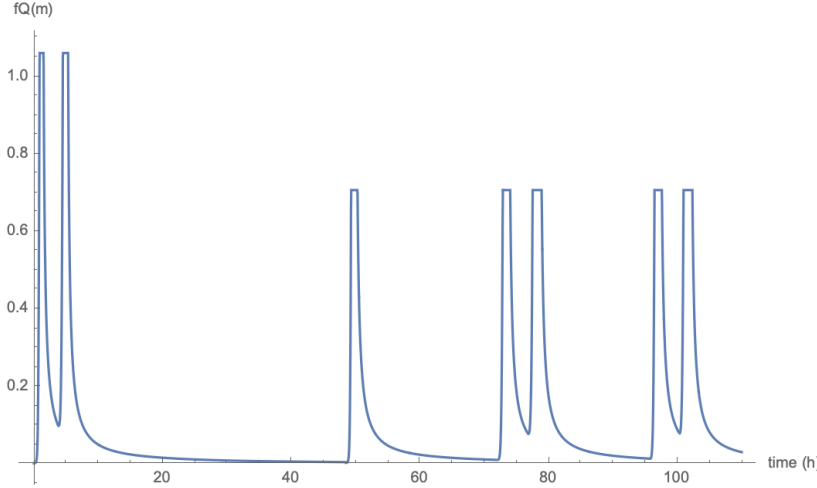

Figure 4-1. Bucket model predictions of the function, $f_Q(t) = Q(t)/S(t)$, for the sequence of seven storms simulated during the 2009 biofilter experiments.

As illustrated in Figure 4-1, the function, $f_Q(t)$, is highly oscillatory, taking on large values during storm events and approaching zero between storms. This oscillatory behavior implies that standard numerical algorithms for integrating $\bar{f}_Q(t)$ are slow to converge and prone to numerical error (results not shown). We resolved this problem by expressing the integral as a rate equation, which was then numerically integrating with the NDSolve command in Mathematica; e.g., the code below took 32 microseconds to evaluate.

```
Clear[fQbar, g];
soln = NDSolve[{g'[x] == fQ[x], g[0] == 0}, g, {x, 0, 110}, MaxStepFraction -> 0.0001];
fQbar[x_] := g[x] /. soln[[1]]

Timing[fQbar[110]]

{0.000032, 12.4892}
```
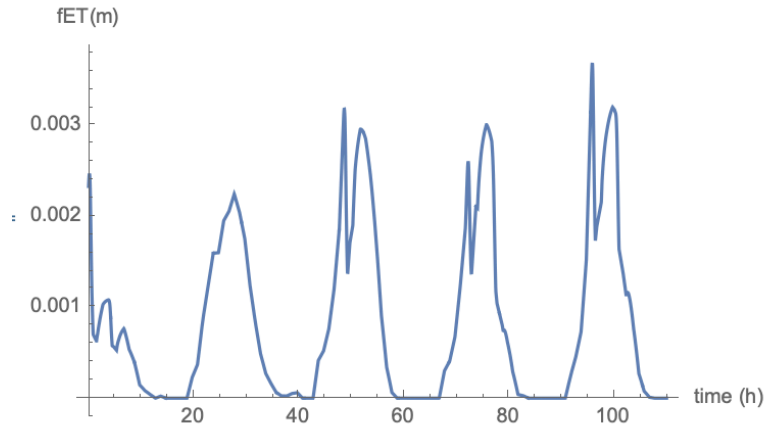
Figure 4-2. The oscillatory behavior of the function, $f_{ET}(t) = ET(t)/S(t)$, *constructed from cPET estimates for our 2019 biofilter experiments (see Text S1), along with bucket model simulations of storage, S(t).*

Likewise, our 2019 time series for the function $f_{ET}(t)$ is highly oscillatory due to diurnal variation in solar radiation and hour-to-hour variations in vapor pressure deficit, cloud cover, and wind (Figure 4-2). We therefore evaluated the function, $\overline{f}_{ET}(t)$ (equation (4-3c)), using the same approach described above; namely, we expressed the integral as a rate equation which was numerically integrated with the NDSolve command in Mathematica; e.g., the Mathematica code illustrated below took 34 microseconds to evaluate.

```
Clear[fETbar, h];
soln2 = NDSolve[{h'[x] == fET[x], h[0] == 0}, h, {x, 0, 110}, MaxStepFraction -> 0.0001];
fETbar[x_] := h[x] /. soln2[[1]]

Timing[fETbar[110]]
{0.000034, 0.0927859}
```

Because infiltration is also highly oscillatory (taking on large positive values during storms, and equal to zero in the periods between storms) the integral term appearing on the right hand side of equation (4-5a) was evaluated using the same approach described above (i.e., expressing the integral as a rate equation and then integrating with the NDSolve command in Mathematica). The Mathematica code below took 88 ms to execute.

7

```
STIntegrationTerm[t_, T_] := Module[{soln, lowerlimit}, Clear[s, lowerlimit];
  If[t - T > 0, lowerlimit = t - T, lowerlimit = 0];
  STsoln = NDSolve[{s'[u] == Exp[-(fQbar[t] - fQbar[u]) - (fETbar[t] - fETbar[u])] j[u], s[lowerlimit] == 0},
    {s}, {u, lowerlimit, t}, MaxStepFraction -> 0.001]; s[t] /. STsoln[[1]]]

Timing[STIntegrationTerm[110, 200]]
{0.088181, 0.112487}
```

The Mathematica code below was used to evaluate the overall solution for age-ranked storage:

```
stUniform[t_, T_, T0_, S0_] :=
  Module[{}, S0 HeavisideTheta[T - t - T0] Exp[-fQbar[t] - fETbar[t]] + STIntegrationTerm[t, T]]
```

Testing the Exact Solution for Age-Ranked Storage. It is easily verified that Equation (4-5a) satisfies the initial condition: $S_T^U(T,0) = S_0 H(T - T_0)$. Next we demonstrate that this solution collapses to total storage when the water age, T, is set to a value larger than the oldest water in storage: $S_T^U(T \geq T_{oldest}, t) = S(t)$. At any time, t, the oldest water in the biofilter is the initial age of the original water in the biofilter (at time $t = 0$) plus the time that has elapsed since the start of the experiment: $T_{oldest} = T_0 + t$. The solution for age-ranked storage was used to calculate the volume of water in the biofilter with age $T = 51 \text{ h} + t$; i.e., one hour than the oldest water in the biofilter, assuming $T_0 = 50$ h (Figure 4-3).

```
Table[{t, stUniform[t, t + 51, 50, 0.054]}, {t, 0, 110, 1}];

ListPlot[%, AxesLabel → {"time (h)", "ST(m)"}]
```


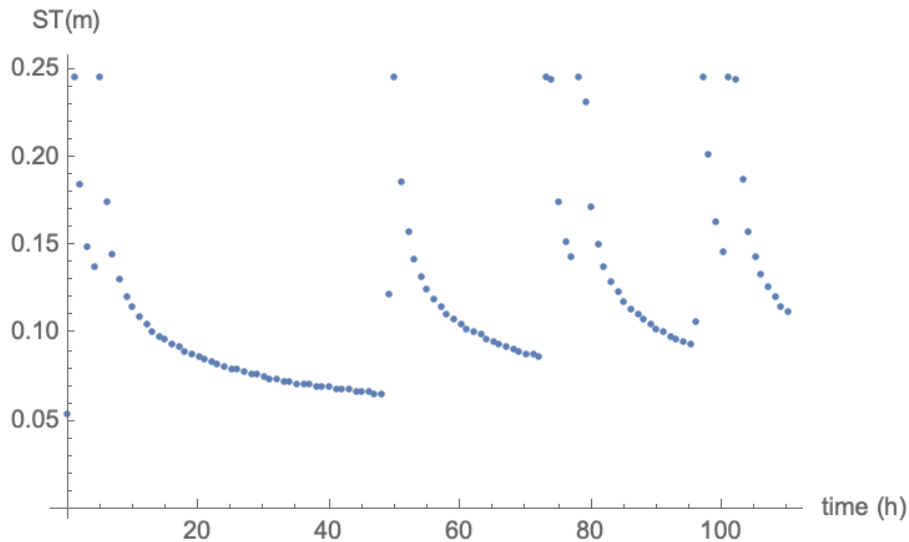_Figure 4-3. Values of age-ranked storage, predicted using equation (4-5a), for the choice of water age older than any water in storage, $T = 51h + t$, where the initial age is $T_0 = 50h$._
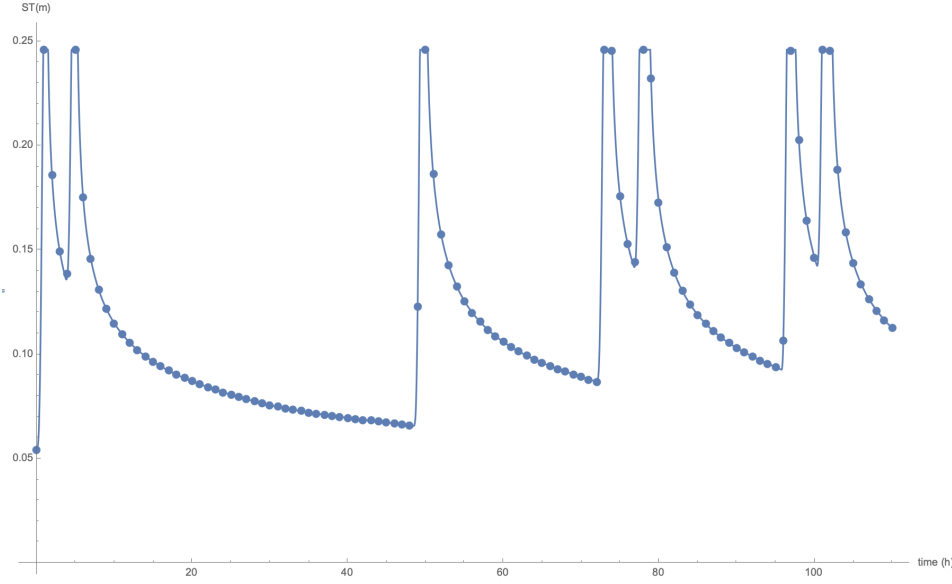
Figure 4-4. Comparison of the age-ranked storage values plotted in Figure 4-3 (points) with the total water volume in storage at any time (S(t), solid line) determined from a bucket model unsteady water balance for the seven storms simulated during the 2019 experiments.

The age-ranked storage predictions align perfectly with the biofilter's time varying water volume (compare points and solid curve in Figure 4-4).

Text S5. Uniform Sampling Predictions for the Age Structure of Water in the Biofilter. The solution for age-ranked storage can be used to evaluate the contribution of individual storms to the evolving age distribution of water stored in the biofilter under uniform selection of the storage for the two outflows (discharge and ET). The residence time distribution (RTD) of stored water in the biofilter, at any time t, can be constructed by normalizing the age-ranked storage by the time varying volume of water in storage (see equation (4b) in the main text) (Harman, 2015):

$$P_{\mathrm{RTD}}^{\mathrm{U}}(T,t) = \frac{S_T^{\mathrm{U}}(T,t)}{S(t)}$$

The corresponding probability density function (PDF) can be obtained by differentiating the CDF form of the RTD with respect to the age variable:

$$p_{\mathrm{RTD}}^{U}(T,t) = \frac{\partial P_{\mathrm{RTD}}^{U}}{\partial T} = \frac{1}{S(t)} \frac{\partial S_{\mathrm{T}}^{U}}{\partial T} \tag{5-1}$$

Combining equations (4-5a) and (5-1) we arrive at the following expression for the PDF form of the biofilter storage RTD under uniform sampling:

9

$$p_{\mathrm{RTD}}^{U}(T,t)=\frac{e^{-\bar{J}_Q(t)-\bar{J}_{\mathrm{ET}}(t)}}{S(t)}\left[S_0\delta(t+T_0-T)+\frac{\partial}{\partial T}\int_a^t e^{\bar{J}_Q(v)+\bar{J}_{\mathrm{ET}}(v)}J(v)dv\right]$$

Taking into consideration the two lower limits for a (see equation (4-5b)) and applying Leibnitz integration rule, the second term in the bracket can be simplified:

$$\frac{\partial}{\partial T}\int_a^t e^{\bar{J}_Q(v)+\bar{J}_{\mathrm{ET}}(v)}J(v)dv=H(t-T)\frac{\partial}{\partial T}\int_{t-T}^t e^{\bar{J}_Q(v)+\bar{J}_{\mathrm{ET}}(v)}J(v)dv=H(t-T)e^{\bar{J}_Q(t-T)+\bar{J}_{\mathrm{ET}}(t-T)}J(t-T)$$

Thus, the PDF form of the biofilter's RTD can be written as follows (compare with equation (7b) in the main text):

$$p_{\mathrm{RTD}}^{U}(T,t)=\delta(t+T_0-T)\frac{S_0}{S(t)}e^{-\bar{J}_Q(t)-\bar{J}_{\mathrm{ET}}(t)}+H(t-T)\frac{J(t-T)}{S(t)}e^{-\bar{J}_{\mathrm{ET}}(t)+\bar{J}_{\mathrm{ET}}(t-T)-\bar{J}_Q(t)+\bar{J}_Q(t-T)} \tag{5-2}$$

The first moment of equation (5-2) yields the expected value, or mean, of the age distribution for water in storage under uniform sampling:

$$\mu_{\mathrm{RTD}}^{U}(t)=\int_0^\infty v\,p_{\mathrm{RTD}}^{U}(v,t)dv \tag{5-3a}$$

$$\mu_{\mathrm{RTD}}^{U}(t)=\left[\frac{S_0}{S(t)}e^{-\bar{J}_Q(t)-\bar{J}_{\mathrm{ET}}(t)}\int_0^\infty T\delta(t+T_0-T)dT+\int_0^\infty TH(t-T)\frac{J(t-T)}{S(t)}e^{-\bar{J}_{\mathrm{ET}}(t)+\bar{J}_{\mathrm{ET}}(t-T)}e^{-\bar{J}_Q(t)+\bar{J}_Q(t-T)}dT\right] \tag{5-3b}$$

The first integral on the righthand side of equation (5-3b) can be simplified after applying the combing property of the Dirac Delta function:

$$\int_0^\infty T\delta(t+T_0-T)dT=t+T_0$$

Furthermore, the Heaviside function appearing in the second integral can be removed as follows:

$$\int_0^\infty TH(t-T)\frac{J(t-T)}{S(t)}e^{-\bar{J}_{\mathrm{ET}}(t)+\bar{J}_{\mathrm{ET}}(t-T)}e^{-\bar{J}_Q(t)+\bar{J}_Q(t-T)}dT=\frac{1}{S(t)}\int_0^t(t-u)J(u)e^{-\bar{J}_{\mathrm{ET}}(t)+\bar{J}_{\mathrm{ET}}(u)}e^{-\bar{J}_Q(t)+\bar{J}_Q(u)}du$$

Back substituting these results into equation (5-3b) we arrive at the final expression for the mean RTD under uniform storage selection (equation (7c) in the main text):

$$\mu_{\mathrm{RTD}}^{U}(t)=\frac{1}{S(t)}\left[S_0e^{-\bar{J}_Q(t)-\bar{J}_{\mathrm{ET}}(t)}(t+T_0)+\int_0^t(t-u)J(u)e^{-\bar{J}_{\mathrm{ET}}(t)+\bar{J}_{\mathrm{ET}}(u)}e^{-\bar{J}_Q(t)+\bar{J}_Q(u)}du\right] \tag{5-3c}$$

Equation (5-3c) was numerically implemented by expressing the integral as a rate equation (see earlier) in Mathematica as follows:

```
Clear[MeanIntegral, q1, MeanIntegralSoln];
MeanIntegral[t0_] :=
 Module[{t = t0},
   MeanIntegralSoln = NDSolve[{q1'[u] == (t - u) j[u] Exp[fQbar[u] - fQbar[t] + fETbar[u] - fETbar[t]], q1[0] == 0},
     q1, {u, 0, t}, MaxStepFraction -> 0.0001];
   q1[t] /. MeanIntegralSoln[[1]]]

meanRTD[t_, T0_, S0_] := (1/storage[t]) (S0 Exp[-fQbar[t] - fETbar[t]] (t + T0) + MeanIntegral[t])
```

Text S6. Uniform Selection Predictions for Solute Concentration in Gravitational Discharge

Our solution for age-ranked storage under uniform selection can also be used to calculate the

concentration of a reactive solute in the biofilter outflow, $C_Q(t)$, by convolving the PDF form of the

backward TTD with the concentration of solute, $C_J(t_i,T)$, that entered the biofilter at time, $t=t_i$, and left

the biofilter as discharge at age T (Harman, 2015):

$$C_Q(t)=\int_0^t C_J(t-T,T)\bar{p}_Q(T,t)dT \tag{6-1a}$$

If the solute in question undergoes first-order reaction (with rate constant k) in the biofilter, the function

$C_J(t_i,T)$ takes on the following form:

$$C_J(t_i,T)=C_J(t_i)e^{-kT} \tag{6-1b}$$

Substituting equations (5-2) and (6-1b) into equation (6-1a) we arrive at the following solution for solute

concentration in water discharged from the biofilter:

$$C_Q(t)=\int_0^t C_J(t-T)e^{-kT}\delta(t+T_0-T)\frac{S_0}{S(t)}e^{-\bar{f}_Q(t)-\bar{f}_{ET}(t)}dT+\int_0^t C_J(t-T)e^{-kT}H(t-T)\frac{J(t-T)}{S(t)}e^{-\bar{f}_{ET}(t)+\bar{f}_{ET}(t-T)-\bar{f}_Q(t)+\bar{f}_Q(t-T)}dT$$

From the combing property of the Dirac Delta, and letting C_0 represent the solute concentration in

"original water", the first integral simplifies a follows:

$$\int_0^t C_J(t-T)e^{-kT}\delta(t+T_0-T)\frac{S_0}{S(t)}e^{-\bar{f}_Q(t)-\bar{f}_{ET}(t)}dT=C_0\frac{S_0e^{-k(t+T_0)-\bar{f}_Q(t)-\bar{f}_{ET}(t)}}{S(t)}$$

The Heaviside function appearing in the integrand of the second integral can be removed:

$$\frac{1}{S(t)}\int_0^t C_J(t-T)e^{-kT}H(t-T)J(t-T)e^{-\bar{f}_{ET}(t)+\bar{f}_{ET}(t-T)}e^{-\bar{f}_Q(t)+\bar{f}_Q(t-T)}dT=\frac{1}{S(t)}\int_0^t C_J(t-T)J(t-T)e^{-kT-\bar{f}_{ET}(t)+\bar{f}_{ET}(t-T)-\bar{f}_Q(t)+\bar{f}_Q(t-T)}dT$$

Thus, solute concentration discharged from the biofilter, assuming uniform sampling, first-order decay in

the biofilter, and no solute mass in the original water, becomes equal to equation (6-2) (compare with

equation (8c) in the main text):

$$C_Q(t) = C_0 \frac{S_0 e^{-k(t+T_0)-\bar{J}_Q(t)-\bar{J}_{\mathrm{ET}}(t)}}{S(t)} + \frac{1}{S(t)} \int_0^t C_J(u) J(u) e^{-k(t-u)-\bar{J}_{\mathrm{ET}}(t)+\bar{J}_{\mathrm{ET}}(u)-\bar{J}_Q(t)+\bar{J}_Q(u)} \, du \qquad (6\text{-}2)$$

To tailor this equation to the 2018 and 2019 bromide pulse experiments, we can express the inflow concentration as follow, where $C_{J,m}$, $t_{m,s}$, and $t_{m,e}$ are the m-th storm's bromide concentration, start time and end time, respectively, and the sum is taken over all N storms where t_i is the entry time of a water parcel exiting the biofilter with gravitational discharge at time t :

$$C_J(t_i) = \sum_{m=1}^N C_{J,m} H(t_i - t_{m,s}) H(t_{m,e} - t_i) \qquad (6\text{-}3)$$

Substituting equation (6-3) into equation (6-2), setting $C_0 = 0$ (reflecting the fact that there was no bromide present in the biofilter's original water during the field experiments), and using the distributive property of integration we obtain:

$$C_Q(t) = \frac{1}{S(t)} \sum_{m=1}^N C_m \int_0^t H(u - t_{m,s}) H(t_{m,e} - u) J(u) e^{-k(t-u)-\bar{J}_{\mathrm{ET}}(t)+\bar{J}_{\mathrm{ET}}(u)-\bar{J}_Q(t)+\bar{J}_Q(u)} \, du \qquad (6\text{-}4\text{a})$$

The Heaviside functions inside the integral can be removed as follows:

$$\int_0^t H(u - t_{m,s}) H(t_{m,e} - u) J(u) e^{-k(t-u)-\bar{J}_{\mathrm{ET}}(t)+\bar{J}_{\mathrm{ET}}(u)-\bar{J}_Q(t)+\bar{J}_Q(u)} \, du = \int_{t_{m,s}}^{t_{m,e}} J(u) e^{-k(t-u)-\bar{J}_{\mathrm{ET}}(t)+\bar{J}_{\mathrm{ET}}(u)-\bar{J}_Q(t)+\bar{J}_Q(u)} \, du$$

Substituting this last result into equation (6-4a) and setting $k = 0$ (because we assume that bromide behaves conservatively) we arrive at the following expression for the outflow concentration (compare with equations (9b) and (9c) in the main text):

$$C_Q(t) = \frac{1}{S(t)} \sum_{m=1}^N C_{J,m} H(t - t_{m,s}) \int_{t_{m,s}}^b J(u) e^{-\bar{J}_{\mathrm{ET}}(t)+\bar{J}_{\mathrm{ET}}(u)-\bar{J}_Q(t)+\bar{J}_Q(u)} \, du \qquad (6\text{-}4\text{b})$$

$$b = \begin{cases} t, & t < t_{m,e} \\ t_{m,e}, & t \geq t_{m,e} \end{cases} \qquad (6\text{-}4\text{c})$$

For example, during the 2019 experiments there was one storm that was spiked with bromide. Hence, in this case $N = 1$ and our solution simplifies as follows, where the bromide addition occurred on the third storm, $m = 3$:

$$C_Q(t) = H(t - t_{3,s}) \frac{C_{J,3}}{S(t)} \int_{t_{3,s}}^b J(u) e^{-\bar{J}_{\mathrm{ET}}(t)+\bar{J}_{\mathrm{ET}}(u)-\bar{J}_Q(t)+\bar{J}_Q(u)} \, du \qquad (6\text{-}5\text{a})$$

$$b = \begin{cases} t, & t < t_{3,e} \\ t_{3,e}, & t \geq t_{3,e} \end{cases} \qquad (6\text{-}5\text{b})$$

The Mathematica code for implementing equation (6-5a) involves two steps; first numerically evaluating the integral and then evaluating the concentration in gravitational discharge from the biofilter at any time:

```
CQConc[t0_, k0_, ts_, te_, c0_] := Module[{t = t0, k = k0, lowerlimit = ts, upperlimit}, If[t < lowerlimit, Return[0]];
    Clear[r];
    If[t < te, upperlimit = t, upperlimit = te];
    integralsoln = NDSolve[{r'[u] == Exp[-k t - fETbar[t] - fQbar[t] + k u + fETbar[u] + fQbar[u]] j[u], r[lowerlimit] == 0},
        {r}, {u, lowerlimit, upperlimit}, MaxStepFraction -> 0.001];
    c0 r[upperlimit] / storage[t] /. integralsoln[[1]]]
```

Text S7. Experimental Approaches for Estimating Lateral Exfiltration from the Biofilter Test Cell

A summary of the process we used to estimate key parameters for the Hydrus 1D and bucket model water balance calculations is presented in Figure S4. One of the key parameters is the fraction of the inflow volume that is routed to the outflow tank. During the set of experimental storms simulated in the summers of 2018 and 2019 we measured time series of the inflow, $I(t)$ [L T^{-1}], to the biofilter and time series of the gravitational discharge from the biofilter routed to the outflow tank (see Figure 1c in the main text), $Q_{\text{outflow}}(t)$ [L T^{-1}]. We know from volume balance (accounting for the fact that ET was a negligible component of the biofilter's overall water balance, see Table S1) that not all inflow to the biofilter was routed to the outflow tank. We therefore let the fixed constant, α, represent the fraction of total gravitational discharge $Q(t)$ routed to the outflow tank: $Q_{\text{outflow}}(t) = \alpha Q(t)$. We determined α using two different approaches: (1) a steady-state experiment conducted during the summer of 2018; and (2) an analysis of the fraction of inflow volume recovered at the outflow tank for transient experimental storms simulated during the summers of 2018 and 2019. These two approaches are described next.

In the first approach, we conducted an experiment in July 2018 (using the same tank and scale experimental set-up described in Section 3.1 main text) in which we supplied a steady inflow of water to the ponding zone of the biofilter (10.1 L/min; the inflow tank was modified to maintain constant head) and simultaneously measured the outflow rate at the outflow tank. The outflow rate eventually stabilized at 5.6 L/min, implying a recovery of $\alpha = 0.55$.

The second approach involved, for each experimental storm in 2018 and 2019, calculating the total volume collected at the outflow tank and dividing it by the total volume of inflow delivered to the biofilter to obtain the storm's "volume recovery fraction". The volume recovery fraction values thus obtained increase inversely with antecedent dry period (ADP) ($R^2=0.82$, Figure S1), presumably because more of the inflow water went to increasing storage during storm events with longer ADPs. By this logic, extrapolating the fractional volume recovery back to an ADP of zero hours should yield the fraction of inflow routed to the outflow tank (under the assumption that none of the inflow water is going toward

increasing storage when the ADP is zero). When this exercise is carried out for the set of storm experiments conducted during the summer of 2018 and 2019 we obtain a y-intercept of $\alpha = 0.46 \pm 0.04$ (Figure S1), which compares closely with the average volume recovery estimated during the steady-state experiments described above ($\alpha = 0.55$, see red horizontal line in Figure S1).

Text S8. Correcting the Time Stamps of Measured Outflow Rate and Bromide Breakthrough
Water leaving our biofilter through the underdrain had to flow by gravity down a manifold to an underground sump where it was pumped into the outflow tank (see Figure 1c in the main text). Our modeling framework was applied to a control volume that included the biofilter media. Consequently, in comparing model predictions measurements of volume and bromide concentration at the outflow tank, we needed to account for the time it takes water to transit from the biofilter underdrain to the outlet tank. We estimated this travel time experimentally by setting up a steady inflow of bromide-free water to the biofilter (using the constant head approach described in the last section). Once steady-state flow had been achieved we poured ~1L of bromide solution (NaBr dissolved in water) into the lateral connecting the biofilter's underdrain to the manifold. Water samples were collected at the outflow collection tank every minute for 14 minutes and measured for bromide concentration using an Orion bromide electrode (Thermo Fisher Scientific, Waltham, MA). From the bromide breakthrough curve, we estimated that the travel time from the biofilter underdrain to the outlet tank is about 3 – 12 minutes. As shown in Figure S5, our simplified infiltration model tended to over-estimate infiltration rates into the biofilter during the Filling Phase, and consequently the bucket model predictions for gravitational discharge tended to lead the gravitational discharge predicted by Hydrus 1D by about 15 minutes. Taking these two factors into account—the overly fast response of the bucket model's gravitational discharge predictions and the time delay associated with water transiting from the underdrain to the outflow tank—we adjusted timestamps of the measured outflow rate and bromide breakthrough curves backwards by about 30 minutes. After time-adjustment, our measurements of flow and bromide concentration at the outflow tank aligned nearly perfectly with the Hydrus and age-conservation predictions of outflow rate and bromide concentration, respectively (see Figures 3 and 4 in the main text).

Text S9. Key Differences in the Experiments Conducted in the Summers of 2018 and 2019
Bromide tracer experiments conducted during the summers of 2018 and 2019 differed in several respects.

First, all of the 2018 storm events were carried out with tap water while, with one exception, all of the 2019 storm events were carried out with stormwater runoff from OCPW's LID campus that had been captured and stored in an 80,000 gallon underground cistern (StormCapture® System, Oldcastle Infrastructure, Inc., Atlanta, GA). The exception was the bromide-spiked third storm event in 2019, which

consisted of a 50:50 mixture of stormwater from the underground cistern and raw sewage from the local wastewater treatment plant (Orange County Sanitation District). The transition from tap water (in 2018) to stormwater (+/- sewage) (in 2019) was motivated by a desire to evaluate the removal of common stormwater contaminants (including heavy metals, nutrients, and microbial pathogens) under transient flow conditions, to be described in subsequent publications.

Second, averaged across all 2018 experimental storm events, ~ 50% of the water added to the biofilter was recovered at the outlet tank (see Text S6). As evapotranspiration (ET) was a relatively minor component of the overall water balance (<1%, see Table S1) we suspected that water was escaping the biofilter test cell into adjacent cells or the surrounding soil; i.e., exfiltration was occurring. Following the 2018 experiments and about five months prior to the 2019 experiments, we removed all plants from the biofilter, excavated the media and discovered that, when the test cell was originally constructed, the contractor had drilled a ca., 5 cm diameter hole into the base of the cinderblock wall separating our test cell from the adjacent cell to accommodate a buried irrigation water supply pipe. The hole was partially sealed (to the extent possible while leaving the irrigation supply pipe in place), the media was replaced, and the biofilter was replanted with a native sedge, *Carex spissa*, recommended for biofilters in southern California (County of San Diego, 2014).

Third, the operation of the control valve differed over the two years. In 2018, storms consisted of tap water and the discharge rate from the inflow tank through the control valve was continuously adjusted with a real-time control algorithm based on continuous measurements of water level in the inflow tank. This set-up could not be replicated in 2019, because the 50:50 mixture of stormwater and sewage applied during the third storm required vigorous mixing of the inflow tank, which interfered with the water level sensor. Consequently, during the 2019 experiments we operated the control valve manually, according to a schedule that roughly conformed to the design storm hydrograph. The storm hydrographs (estimated by differentiating the measured decline in weight of the inflow tank over time) generated using this approach compare reasonably well to the design storm, although the peak flow is reduced in both years, and the storm hydrographs in 2019 are smoother and more reproducible from storm-to-storm (Figure S2).

References

Aerts, R., de Caluwe, H., & Konings, H. (1992). Seasonal allocation of biomass and nitrogen in four *Carex* species from mesotrophic and eutrophic fens as affected by nitrogen supply. *Journal of Ecology, 80*(4), 653-664.

Allen, R. G., Pereira, L. S., Raes, D., & Smith, M. (1998). Crop evapotranspiration – Guidelines for computing crop water requirements – FAO Irrigation and Drainage Paper 56. Food and Agriculture Organization of the United Nations.

Busch, J., & Losch, R. (1998). Stomatal behavior and gas exchange of Sedges (*Carex* spp.) under different soil moisture regimes. *Physics and Chemistry of the Earth, 23*(4), 443-448.

County of San Diego. (2014). *County of San Diego Low Impact Development Handbook*. San Diego, CA: Department of Public Works, Watershed Protection Program, County of San Diego.

Durner, W., & Iden, S. C. (2011). Extended multistep outflow method for the accurate determination of soil hydraulic properties near water saturation. *Water Resources Research, 47*(8), W08526.

Harman, C. J. (2015). Time-variable transit time distributions and transport: Theory and application to storage-dependent transport of chloride in a watershed. *Water Resources Research, 51,* 1-30.

Le Coustumer, S., Fletcher, T. D., Deletic, A., Barraud, S., & Poelsma, P. (2012). The influence of design parameters on clogging of stormwater biofilters: A large-scale column study. *Water Research, 46*(20), 6743-6752.

Lindsey, G., Roberts, L., & Page, W. (1992). Inspection and maintenance of infiltration facilities. *Journal of Soil and Water Conservation, 47*(6), 481-486.

Mallants, D., Mohanty, B. P., Vervoort, A., & Feyen, J. (1997). Spatial analysis of saturated hydraulic conductivity in a soil with macropores. *Soil Technology, 10*(2), 115-131.

Mapa, R. B., Green, R. E., & Santo, L. (1986). Temporal Variability of Soil Hydraulic Properties with Wetting and Drying Subsequent to Tillage. *Soil Science Society of America Journal, 50*(5), 1133-1138.